Journal of Molecular Graphics and Modelling 29 (2010) 266–279

Contents lists available at ScienceDirect

Journal of Molecular Graphics and Modelling

journal homepage: www.elsevier.com/locate/JMGM

A coarse-grained molecular model for actin–myosin simulation

William R. Taylor*, Zoe Katsimitsoulia

Division of Mathematical Biology, MRC National Institute for Medical Research, The Ridgeway, Mill Hill, London NW7 1AA, UK

ARTICLE INFO

Article history:
Received 9 March 2010
Received in revised form 15 June 2010
Accepted 15 June 2010
Available online 3 July 2010

Keywords:
Actin
Myosin
Molecular motor
Brownian dynamics

ABSTRACT

We describe a very coarse-grained molecular model for the simulation of myosin V on an actin filament. The molecular representation is hierarchical with the finest level representing secondary structure elements (end-points) which are grouped into domains which are then grouped into molecules. Each level moves with a Brownian-like motion both in translation and rotation. Molecular integrity is maintained by steric exclusion and inter-domain restraints. A molecular description is developed for a myosin dimer on a actin filament with binding interactions also specified between domains to simulate both loose and tight binding. The stability of the model was tested in the pre- and post-power-stroke conformations with simulations in both states being used to test the preferred binding site of the myosin on the filament. The effects of the myosin twofold symmetry and the restriction of an attached cargo were also tested. These results provide the basis for the development of a dynamic model of processive motion.

1. Introduction

Motion within the eukaryotic cell is based on a protein motor moving along a polymer track. In some situations, the polymer might be nucleic acid and the motor a polymerase or a helicase or even the ribosome but more generally, cell motility employs either kinesin or dynein moving along a microtubule (an α/β tubulin polymer) or myosin on an actin filament (an F-actin polymer). With their employment in muscle, the actin–myosin system is by far the most abundant motor in higher organisms but it also has great diversity, as is reflected in the many different sub-types of myosin. For example, actin–myosin motors are employed for the transport of vesicles inside the cell using double-headed motors or with motors arranged in arrays they can power large scale motion, as seen in muscle or in the invasion of the red-blood by the malarial parasite. The former type of motion, in which the motor undergoes multiple chemical cycles before detaching, is referred to as processive, in contrast to the motion of filaments along a bank of static motors [1–4].

The operation of muscle myosin (myosin-II) has been extensively studied over many years and more recently, X-ray and electron based structures have been solved for almost every stage in the myosin motive cycle. Processive myosins typically transport cargo inside the cell, either forward (e.g. myosin-V) or backwards (myosin-VI) relative to the actin filament direction and are less well studied, with X-ray structures having only recently been solved. While these structures show the details of the molecule, they indicate little about the coordination of motion (if any) between the paired motors. Information on this aspect comes either from biophysical studies or electron microscopy. The latter can provide snap-shots but no dynamics while the former can provide information on dynamics but without atomic scale visualisation.

All studies point to an ATP-driven mechanical cycle common to all myosin motors. This, arbitrarily, begins with the ATP bound myosin free of actin. With ATP hydrolysis, the myosin can bind to actin but retains the hydrolysis products, ADP and inorganic phosphate (Pi). With the release of Pi, the myosin undergoes a large conformation change associated with motion, called the "power-stroke" in which the main catalytic and actin binding domain swings through a large angle relative to its fixed point of attachment at the opposite end of the molecule. This tight-binding conformation, called the "rigor" state, is retained until ADP is released and with ATP binding, the myosin dissociates from actin and the cycle repeats. This cycle is shown in the context of the two chains of a myosin-V dimer in Fig. 1.

An approach to synthesise the structural data with kinetic data is through a molecular model. However, a double-motor myosin, with a track of actin to run along, constitutes a very large system which would be far too big to simulate at the atomic level using molecular dynamics, except perhaps on the worlds largest supercomputers. This has led to the development of course-grained (CG) models in which groups of atoms, or residues, are represented by a single point. Through such reductions it is hoped that simulations of a useful length can be run on moderate computers without having reduced the molecular representation to a level at which high-resolution structural information has been lost [5–7].

In this work we develop a multi-level CG molecular model for myosin-V on actin that employs a hierarchy of three structural lev-

* Corresponding author. Tel.: +44 208 8162298; fax: +44 208 8182460.
E-mail address: wtaylor@nimr.mrc.ac.uk (W.R. Taylor).

1093-3263/$ – see front matter © 2010 Elsevier Inc. All rights reserved.
doi:10.1016/j.jmgm.2010.06.004

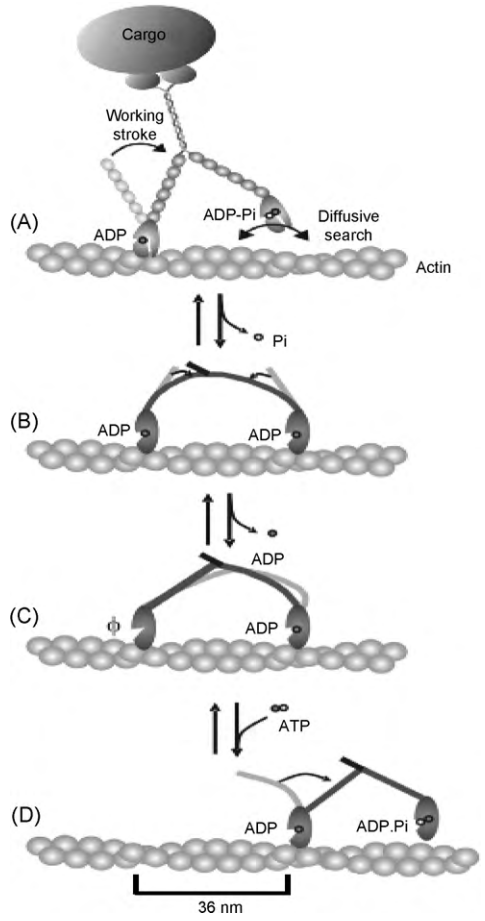

Fig. 1. Myosin-V ATP cycle. (a) With release of Pi, the left leg makes a power stroke allowing the right leg to search for an actin binding site. (b) The bound right leg binds and loses its Pi, creating strain in the legs (arrows). (c) With loss of ADP in the left leg, the power stroke can progress in the right leg. (d) On ATP binding, the left leg is released from actin and swings to the right and with ATP hydrolysis, it to returns to the pre-power-stroke conformation. (Reproduced from [21], with permission.)

els. At the lowest level, each secondary structure element (SSE) is represented as a cylinder. These are then grouped into domains which, in turn, are grouped into individual proteins. Elements at all levels move with a simple Brownian-like motion and collide with each other, however, lower-level elements do not interact between groups unless their parent groups have collided. This hierarchy of interaction is applied recursively across all the proteins in the simulation using the efficient collision-detection algorithm in the graphical programming language Java3D [8].

2. Methods

2.1. Myosin model

The molecular structure of myosin-V (PDB code: 2DFS [9]) consists of two heavy-chains, of over 1000 residues each, linked by a 130 residue length of coiled-coil at their carboxy-terminal ends (Fig. 2(a)). The globular amino-terminal motor domain extends into a long α-helix which, at regular intervals, is bound by six calmodulin-like light-chains (Fig. 2(b)). This region consists of repeated binding sites called "IQ" motifs to which the light-chains bind. The molecular structure shown in Fig. 2 is in the "resting" state where the carboxy terminus is bound back to the amino terminus (by unresolved domains) preventing any motion. When cargo is bound to the carboxy-terminal coiled-coil, the motor domains become free to bind to actin and begin moving. Excluding the coiled-coil segment, the two heavy-chains (referred to below as "legs") have a close, but not exact twofold symmetry. In anthropomorphic terms, the molecule must therefore walk having two left (or right) legs and, given that each globular motor or "foot" domain,[1] binds actin with the same orientation, then some interesting gymnastics must result.

Taking the coordinates of the myosin-V structure (2DFS), secondary structure elements (SSEs) were defined using the `stick` program that identifies all linear segment in a protein α-carbon backbone and establishes their end-points based on the minimum moment of inertia about each line, summed over all lines [10]. This method is not sensitive to details of hydrogen-bonding and can provide robust secondary structure definitions on models and low-resolution structures, such as 2DFS which has a nominal resolution of 24 Å (Fig. 2(c) and (d)).

2.1.1. Domain assignment in the 'foot'

The foot-domain (residues 1–770 in 2DFS) was analysed for sub-domains that could form the basis of a structural hierarchy. However, an automatic method [11] with default settings split the molecule only into two parts. The single parameter in this method that controls the granularity of the domains (`spread`) was reduced to 10, generating the finer division into six domains shown in Fig. 3. This separated the core β/α ATPase domain of the molecule along with three domains that form the ATP-binding cleft, two of which interact with actin, and two domains, including the all-β SH3 domain at the N-terminus and the mainly-α domain at the C-terminus that leads into the long light-chain binding helix. The latter two domains are central to the leg/foot bending motion of the molecule and will be referred to jointly as "ankle" domains. These domains correspond reasonably with those identified originally by 'eye' [12] and have some correspondence to units identified by normal mode analysis on myosin-II [13].

Five of the six domains range from 50 to 100 residues with the core β/α domain over 200 residues. A similar distribution of sizes was also seen in the number of SSEs and, although a structural hierarchy in our simple Brownian dynamics method [8] can be imbalanced, for computational reasons, we preferred that each level in the hierarchy should contain an equal number of between 10 and 20 components. To equalise the size of the domains at the secondary structure level, some small secondary structure elements were removed from the fringes and the core domain was split into two halves. After some 'trading' of secondary structure between adjacent domains, seven domains were defined with six secondary structure elements each and, with some exceptions, these largely preserve their order in the chain and correspond well to the domains defined automatically at the α-carbon level (Fig. 3).

As the myosin foot domains (numbered 1–7) will be referred to frequently, codes that reflect their function were assigned as: the "ankle" domains A1, A2 (1 and 7), the "binding" domains B1, B2 (5 and 6) and the "core" domains C1, C2 and C3 (2, 3 and 4) (Fig. 3(f)). In the terminology commonly used in the muscle literature, these domains correspond as: A1 = SH3, A2 = converter, B1 + C2 + C3 = upper 50 K, B2 + C1 = lower 50 K. The centroids of these domains were then used to define a coordinate reference frame for the foot with the vector in the direction C1 → C3 in the *X* direction, the vector in the direction B2 → C2 in the *Y* direction, the *Z*-axis was defined as orthogonal to *X* and *Y* and the *Y*-axis redefined as orthogonal to *X* and *Z* giving a set of three mutually orthogonal axes forming a right-hand coordinate reference frame. Unit vectors

[1] The parts we refer to here as "leg" and "foot" are more commonly referred to in the muscle literature as "arm" and "head", respectively. However, with the obvious walking behaviour of myosin-V, we will adhere to the names of body parts that are more closely associated with locomotion.

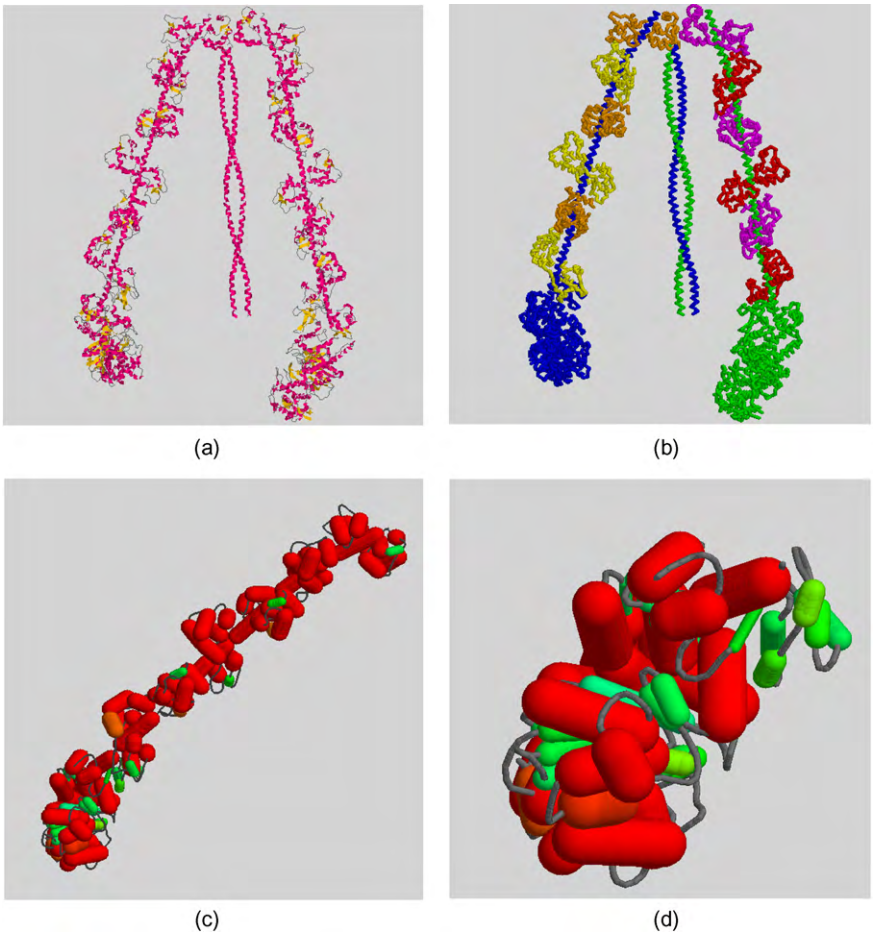

Fig. 2. Myosin-V structure. The structure of dimeric myosin-V (2DFS), determined by single-particle cryo-electron microscopy is shown (a) with secondary structures represented in cartoon style (using RASMOL) with α-helix coloured pink and β-strands yellow. (b) The same structure is shown as a virtual α-carbon backbone with the two heavy chains coloured cyan and green and their associated light-chains in alternating yellow/orange and red/magenta, respectively. Secondary structure line-segments ("sticks") are shown as green tubes for β-strands and thicker red tubes for α-helices. (c) For the full structure of heavy and light chains (excluding the coiled-coil C-terminus) and (d) for the globular foot domain. (The amino-terminus lies in the all-β SH3 domain to the right.)

along these axes constitute a rotation matrix that will be used in geometric operations described below.

2.1.2. Domain assignment in the 'leg'

Domain assignment in the calmodulin-like light-chains that constitute the bulk of the 'leg' is simpler than domain assignment in the foot as each light-chain has two clearly distinguished domains, each consisting of twinned calcium-binding EF-hand motifs. The light-chains used to construct the (2DFS) myosin-V structure all have the same sequence (bar a 2-residue N-terminal truncation in half of them) but fall into two groups: chains B, D, F and C, E, G. All have a within group RMSD under 1 Å, but all cross group RMSDs are over 3.4 Å (Supplementary Fig. 13).

The secondary structures between groups are similar enough to allow a consensus definition over all six chains. However, the differences between domains within all chains are larger than between chains with 4.19 Å/66 and 4.86 Å/68 (RMSD/residues) for the B-chain and C-chain, respectively. The main difference lies in and around the domain linker with the amino terminal domain extending into the linker as an α-helix but continuing into the second domain as an extended chain (where an α-helix is found in the first domain). These differences are summarised in Supplementary Fig. 14 in which the domains have been aligned for both chain types. From this comparison, the ambiguous first helix was assumed to exist in all copies of the domain giving a consensus assignment of the four canonical α-helices associated with the double EF-hand motifs. The two minor β-strands that link the EF-hands were ignored for the moment.

The long extended helix in the heavy-chain, to which the light-chains are bound, packs closely with each light-chain along its length and effectively becomes an integral part of their structure. In terms of a structural hierarchy, it therefore makes more sense to allocate segments of the heavy-chain helix across the light-chain domains. This was done as shown in Fig. 4 for the C-chain. The resulting augmented domains now have five secondary structure elements each, compared to six in the foot sub-domains and to equalise the number of SSEs across all myosin domains, a short β element was reintroduced to represent the bulk of the small β-sheet with end-points lying between the two strands of the sheet.

2.1.3. Hinge motions

2.1.3.1. Ankle bending. The relative movement of the leg and foot does not have a well localised hinge point but involves a combination of complex shifts involving interactions with the two ankle domains (A1 and A2 in Fig. 3(d)). The net effect is that the leg rotates about a virtual centre located close to the middle of the foot [14]. We encoded this literally by placing the foot-domain reference frame at the centroid of the foot and rotating the six light chains (12 domains that include the long heavy-chain helix) around this local *Z*-axis. The accuracy of the molecular interactions brought about by this rotation will be assessed in Section 3 along with the desired degree of rotation.

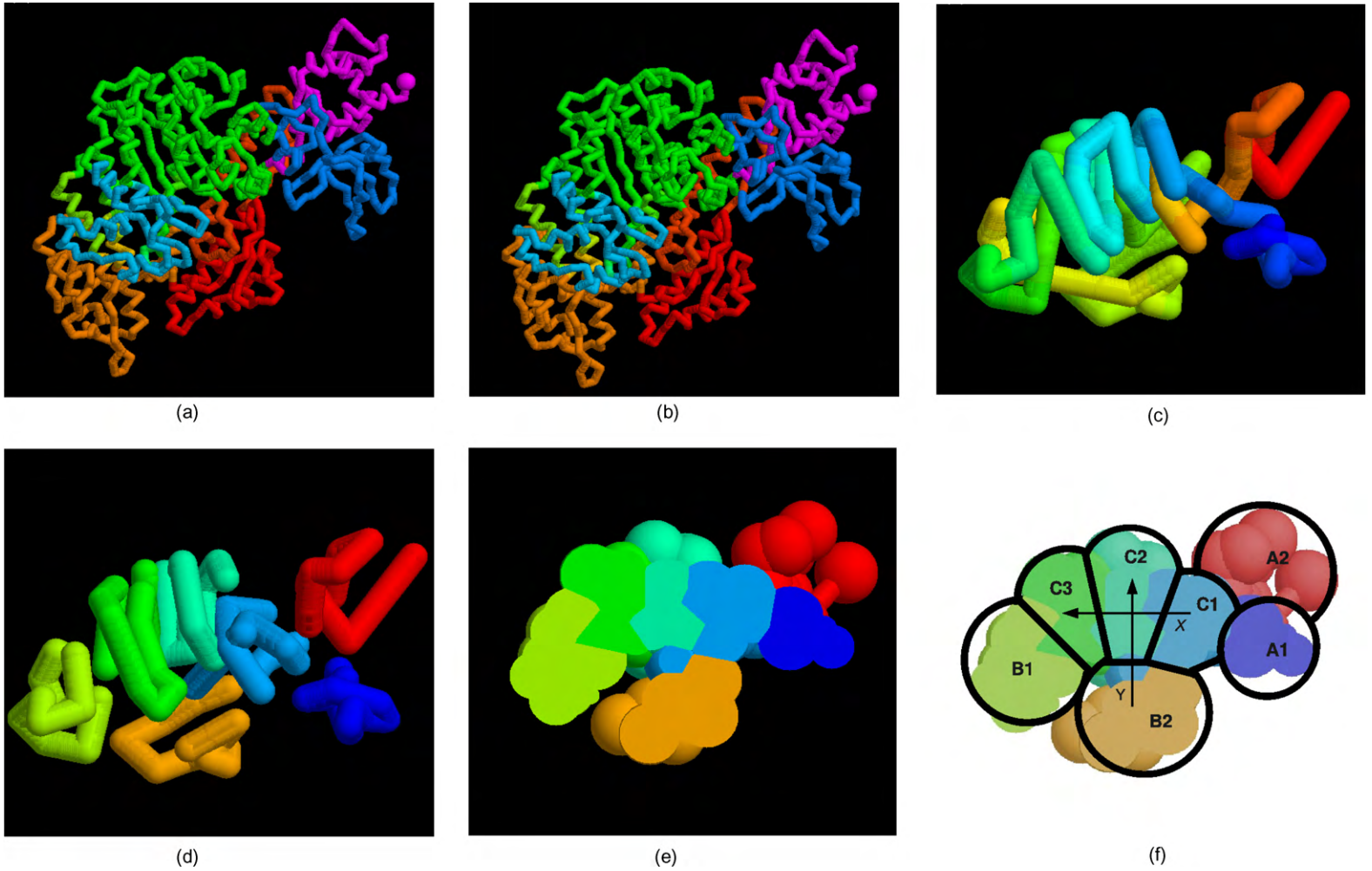

Fig. 3. Myosin foot sub-domain assignments. (a and b) Sub-domains defined within the globular foot domain are identified in different colours on a α-carbon-backbone trace of the chain. The core β/α ATP-binding domain is green, surrounded by two lower domains (red and orange) that are involved in actin binding. The dark-blue and magenta domains form the interface to the light-domains that extend into the "leg". The termini are marked by spheres. (The images are a stereo-pair.) (c) The chain of secondary structure elements (SSEs) is drawn as a continuous tube after removal of small fringe SSEs with blue = amino through to red = carboxy termini. (d) SSEs allocated to produce seven domains: 3 core domains (light-blue, cyan, green), two binding domains (yellow, orange) and two ankle domains (blue, red). (e) The SSEs represented in this figure are redrawn with space-filling spheres placed on each SSE end-point and sliced through by a plane that would also contain the 'leg' extension. (f) As in part (a) but with domain boundaries sketched and domain codes added: A1–2 (ankle), B1–2 (binding) and C1–3 (core). The direction of the *X* and *Y* axes of the reference frame are indicated by arrows. (For interpretation of the references to colour in this figure legend, the reader is referred to the web version of the article.)

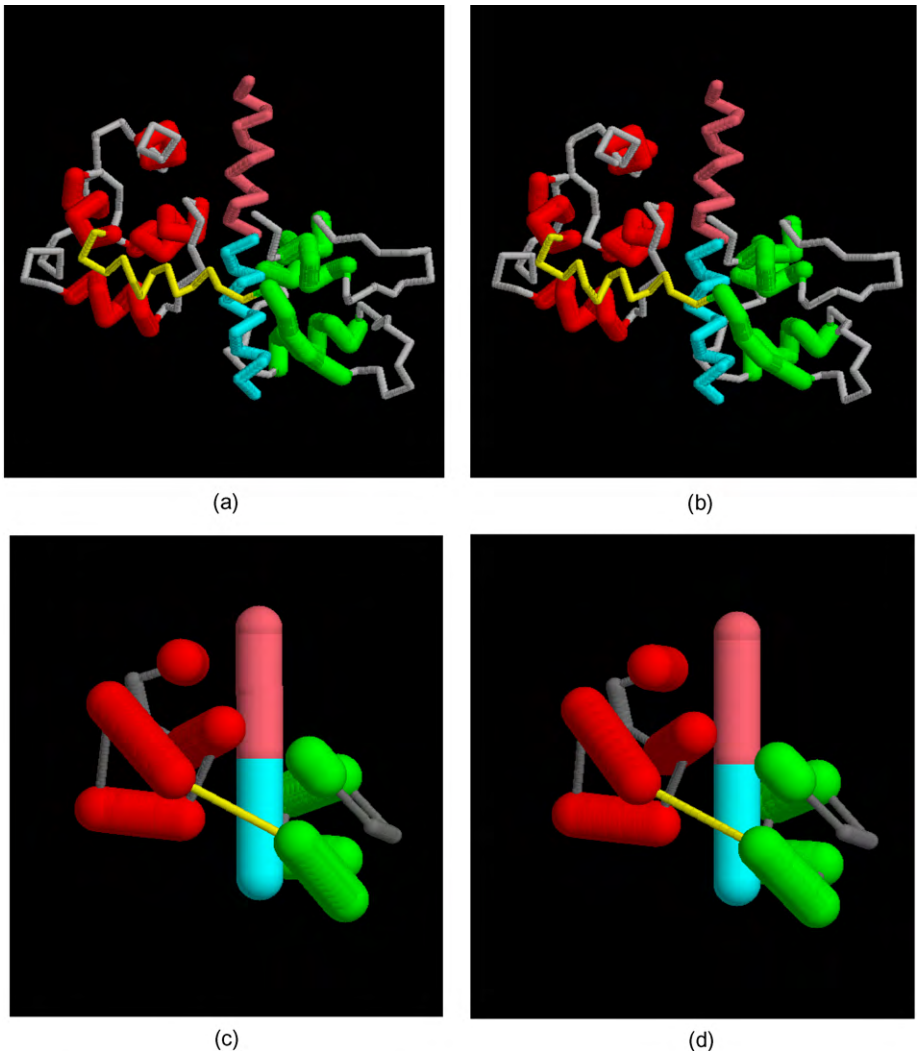

Fig. 4. Myosin light-chain domain structure. (a and b) A light-chain from the myosin-V structure (2DFS, chain C) is shown with the four consensus α-helices coloured red in the amino-terminal domain and green in the carboxy terminal domain. The portion of the heavy chain helix to which the light-chain is bound is shown with the segment allocated to the C-terminal domain coloured cyan and the segment allocated to the N-terminal domain coloured pink. The C-terminus of the heavy-chain helix is at the top and the domain linker segment is yellow. (c and d) The structure shown above is represented as SSE sticks using the same colouring scheme and in the same orientation. The segment representing the short β-sheet is drawn as a thicker grey tube. Both parts are stereo-pairs. (For interpretation of the references to colour in this figure legend, the reader is referred to the web version of the article.)

2.1.3.2. Leg swinging. The relative movement of the two myosin legs was modelled with completely free rotation and also with constraints to impose the twofold relationship between the two heavy-chains. The details of this hinge are also vague as the myosin-V structure is in the "resting" position and has a break in the chain connectivity in the region of the hinge with 41 residues missing. To create specific hinge point for use in computation, we took the last point in each heavy-chain and shifted them to a common mid-point. This was done for two chains sitting in a parallel orientation (both feet aligned) and in an anti-parallel orientation as seen in the myosin-V structure (2DFS). The hinge was maintained in both by shifting one or both end-points back to a common position after the chains had been given a random displacement.

2.2. Actin model

2.2.1. Actin domain assignment

Actin coordinates were taken from the cryo-EM model of insect flight muscle [15] (PDB code: 1O1B, chain 8). Like the myosin-V model, although this has nominally a very low resolution, the component molecules have been assembled from higher resolution structures. Following the myosin analysis, we examined the structure for domains that might provide a natural hierarchy of structure. Using the STICK program with its default parameter, actin divides clearly into two large domains, one of which can be reasonably subdivided into two smaller domains. The other half, however, does not divide so evenly with a large domain (containing the N and C termini) and a smaller fragment (Fig. 5).

Given that simulations may involve a large number of actin molecules, we raised the level of the structural hierarchy by treating two actin monomers as a single molecule with just four domains (the blue and red + green domains in Fig. 5(b)). Conveniently, when reduced to secondary structure line-segments by the STICK program (Fig. 5(c)), each domain had 13 elements (Fig. 5(d)). Each actin domain will be referred to below as F1 and F2 ("F" for filament) with their symmetrical counterparts across the filament axis as F1′ and F2′.

2.2.2. Actin filament construction

The actin dimer units were used to generate an extended filament using the relationship between molecules in the PDB

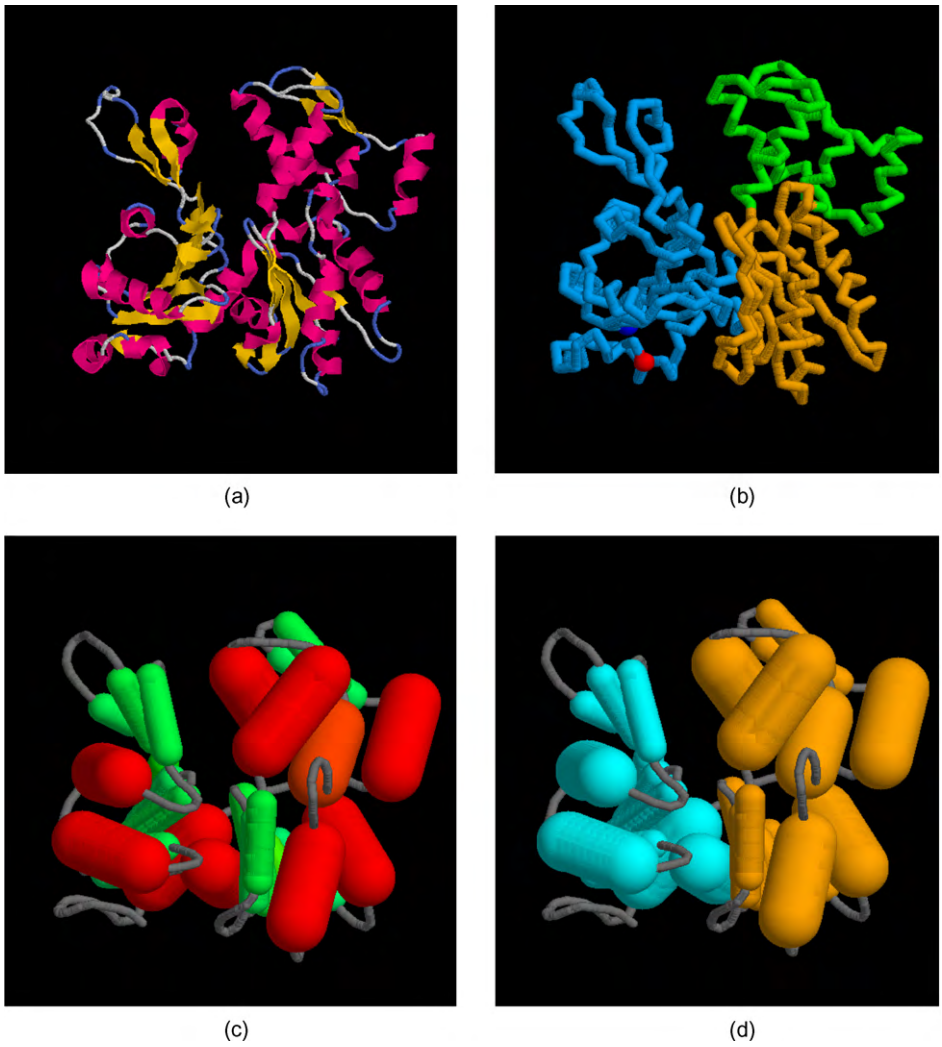

Fig. 5. Actin domain and secondary structure. (a) The structure of actin (PDB code: 1O1B, chain 8) is shown with secondary structures represented in cartoon style (using RASMOL) with α-helix coloured pink and β-strands yellow. (b) The same structure is shown as a virtual α-carbon backbone with major domains in different colours. An additional small fourth domain can be identified (top left). The C-terminus is a red ball with the N-terminus hidden close behind. (c) The secondary structure line segment assignment and (d) coloured as two domains called F1 (left) and F2 (right). (For interpretation of the references to colour in this figure legend, the reader is referred to the web version of the article.)

structure 1O1B. This involves a translation along *Z* of 55 Å combined with a rotation of 28°. As with the myosin foot, we also required a coordinate reference frame for the actin. The obvious choice for one axis is the filament axis (designated *X*) with an orthogonal cross-filament axis (designated *Y*). The orientation of *Y* was set so that it lay in the plane defined by the *X*-axis and the line from the *X*-axis to the centroid of the cyan coloured domain in Fig. 5(d). Although, arbitrary, the choice of this domain orients the *Y*-axis towards the myosin bound in the structure. The *Z*-axis was set orthogonal to both *X* and *Y* creating a right-hand reference frame.

The structure of the actin filament was maintained during simulation by a distance constraint of 55 Å between consecutive dimer centres (which lie on the filament axis) and also by constraints between equivalent domains in adjacent molecules using the slightly larger distance of 58 Å to allow for the longer off-axis separation. Two additional inter-molecular constraints were added to maintain the orientation between subunits: $F1_{i-1}$–$F2_i$, $F1_i$–$F2_{i+1}$, where the subscripts specify sequential actin molecules in the filament. The six intra-molecular links between the four domains in the dimer were also kept close to their ideal initial values.

2.3. Actin–myosin binding

From the position of the actin bound myosin in the insect flight muscle structure (Fig. 6) it can be seen that the main interaction occurs between the myosin foot domain B2 and actin domain F1 (lower-left in Fig. 5(b)) with some less substantial interactions between the loop regions of myosin domain B1 and actin domain F2, in particular with the sub-domain coloured orange in Fig. 5(b).

2.3.1. Loose binding constraints

To model the actin–myosin interaction in a simulation with representation at multiple levels, we took the distance between the centre of the myosin foot domain (close to residue G464) and the centre of the actin dimer (close to the mid-point of X137 and W137) of 63 Å as an ideal high-level separation. This provides only a proximity constraint with no directional component and to introduce some orientation we added a domain-level constraint between the two myosin binding domains (B1, B2) and the actin. Based only on the actin centre, these interactions have little specificity and can be thought of as a general attraction between actin and the myosin binding region and will be referred to below as “loose-binding”.

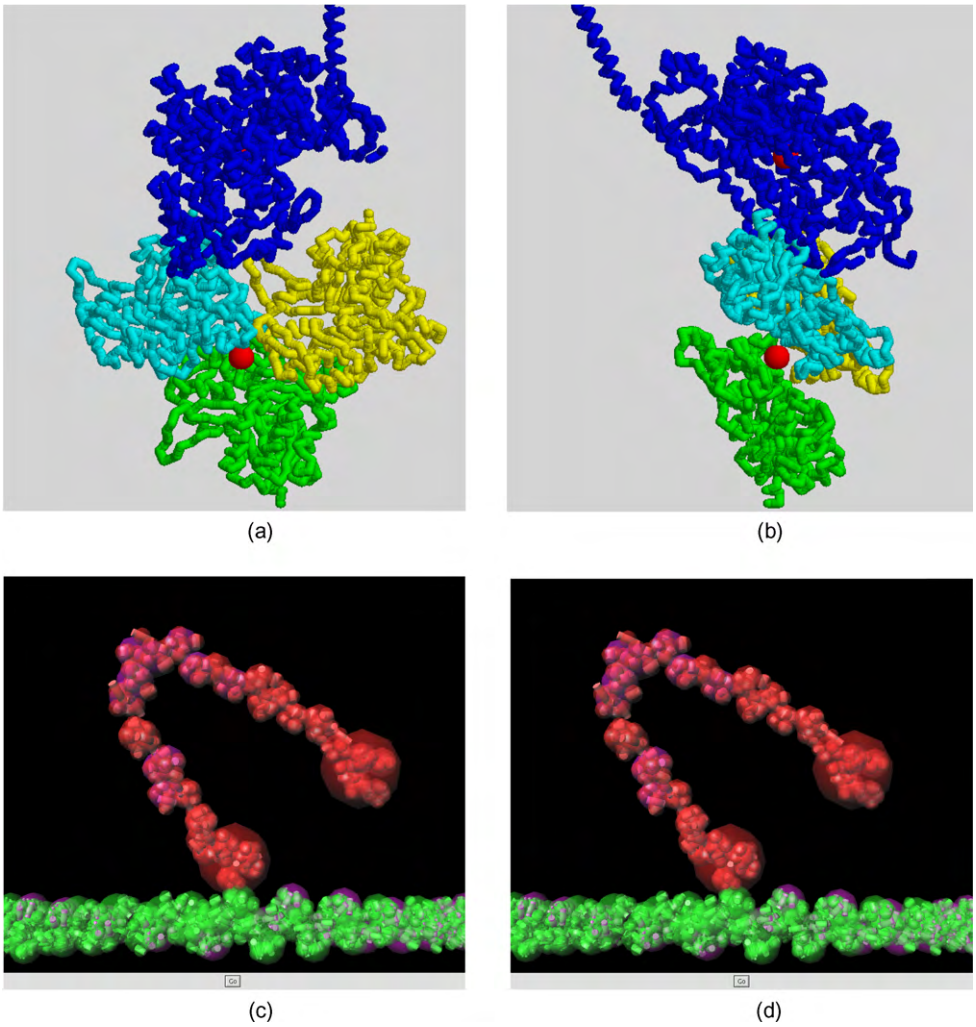

Fig. 6. Actin myosin binding. The structure of myosin bound to actin (PDB code: 1O1B, chains G, W, X, V) showing the myosin heavy-chain (blue) and three actin molecules, two of which (yellow, cyan) lie above the filament axis and the third (green) below. (a) Viewed across the filament axis. (b) Viewed down the filament. The two red spheres mark the centre of the myosin domain and the mid-point of the actin dimer. (c and d) The myosin-V dimer model (red) is shown in its loose-binding state to the actin filament model (green). The actin polarity runs from right (− or 'pointed') to left (+ or 'barbed') so the myosin would "walk" from left to right. Secondary structure elements (SSEs) are depicted as cylinders (with large/small diameters for α/β) connected by fine lines. The translucent spheres show the higher level groupings of SSEs into domains. (For interpretation of the references to colour in this figure legend, the reader is referred to the web version of the article.)

2.3.2. Tight binding constraints

To add stereo specificity to the interaction, including foot alignment, additional domain-level constraints were specified between the myosin binding domains and the bound actin domains (F1 or F1′) in three consecutive molecules: $F1_{i-1}$–B1, $F1_i$–B1, $F1_i$–B2, $F1_{i+1}$–B2, where the subscripts denote sequential actin dimers with *i* being the one to which the myosin is loosely bound at the higher-level. These four constraints specify the centre of the interaction as the $F1_i$ domain and direct the B1–B2 orientation of the myosin foot-domain to align roughly with the actin filament axis direction as seen in the muscle structure. These inter-domain constraints are referred to as "tight-binding".

2.4. Molecular animation

2.4.1. Domain distance constraints

To maintain the internal structure of SSEs within a domain, the distances between each SSE were shifted by 1 Å towards the ideal starting distance whenever the violation exceeded or fell below 1 Å.

For the four actin dimer domains, all six inter-domain distances were constrained as described above but for the larger number of myosin domains there will be systematic movements between the foot and leg that should not be constrained. Inter-domain constraints were therefore only applied within the myosin foot domain and within the leg domain with only two distances constrained between the last myosin domain (7) and the first two light-chain domains.

Repulsion between all layers in the structural hierarchy was determined by the size of the bumping radius associated with each element. For the three levels (SSEs:domain:protein) these were 7.5:15.0:40.0 for myosin and 7.5:20.0:20.0 for actin. All spheres were located at the centroid of their respective level, except for the myosin protein level sphere which was located on the centroid of the foot domain. The protein level sphere for actin was set smaller than expected for the volume of the four domains it contains to prevent excessive computation within the actin filament which is sufficiently constrained by the specific distance constraints described above.

2.4.2. Molecular dynamics

The animation of random motion in the molecular components in the hierarchy was implemented as a rotation and translation applied to each level. The overall degree of motion was set by a parameter `wild` which took a default value of 0.01. This value

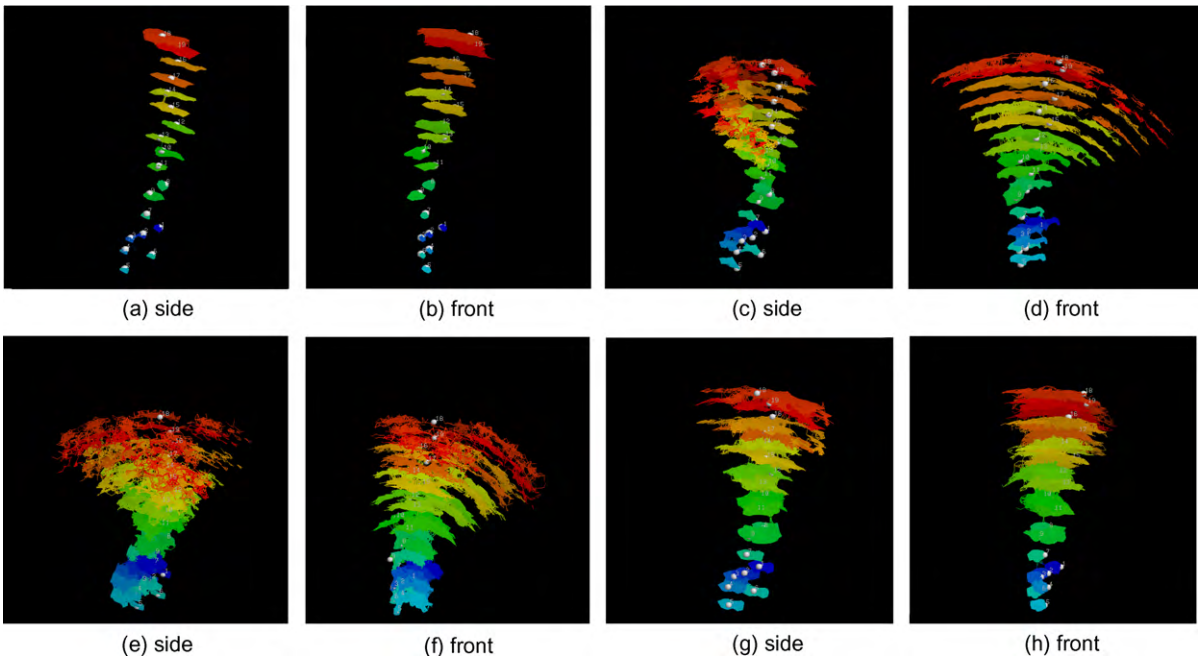

Fig. 7. Myosin ankle flexibility. The myosin domain positions are plotted in the coordinate frame of the foot domain (Section 2.1.1). 1000 coordinate sets are drawn in RASMOL such that neighbouring positions in different molecules become bonded with the resulting meshwork creating an impression of density. Each domain is coloured by sequence (blue to red) and the appearance of layers shows that the domain separations are respected. In the *front* view the foot domain *Z*-axis runs across the page while in the orthogonal *side* view, the *X*–*Y* axes lie at 45° on the page. White spheres mark the starting positions of the domains numbered: 1–7 = foot, 8–19 = leg. (a and b) With wild = 0.01. (c and d) With `wild` = 0.02. In the side views (a and c), the actin filament runs from left (−) to right (+) at a 45° angle. The simulations were then run for 10,000 steps (one frame in 10 is plotted) with (e and f) only local constraints plus a single distance constraint along the length of the leg (domains 9–18) and in (g and h) two constraints from the ankle to the most distant light chain (domains 1–19, 7–18). (For interpretation of the references to colour in this figure legend, the reader is referred to the web version of the article.)

was applied to each axis as a rotation about the centroid in radians picked randomly between ±`wild`. Because large objects will have a bigger peripheral displacement, the value of `wild` was kept constant across levels. Translational displacements were similarly implemented by a random shift between ±`wild` applied to each dimension. Larger objects, however, were given a larger random translational displacement in the ratios 1:2:3 for each level SSE:domain:protein, respectively. For both rotation and translation any transform applied at a high level node was also applied to all objects lying under it in the structural hierarchy. This was efficiently implemented in Java3D as a tree of transform-groups. Fig. 6(c) and (d) shows a visualisation of the hierarchy with the SSEs shown as cylinders and the higher-level groups as translucent spheres.

3. Results

3.1. Myosin ankle flexibility

In the model, inter-domain restraints are continually perturbed by the Brownian-like 'thermal' motion of the domains, the 'temperature' of which is determined by the parameter `wild`. For values of `wild` over 0.02, the restraints are not enforced enough to keep pace with random drift and the molecule becomes distorted. Values under this threshold were investigated over 1000 iteration steps by visualising the leg positions in the common coordinate frame of the foot domain (Section 2.1.1).

With values of `wild` of 0.01 and 0.02, the leg domain remains extended and describes a seemingly random "wobble" largely about the ankle. With `wild` = 0.01 the wobble movement is relatively confined and isotropic compared to the spread seen with `wild` = 0.02 which is more than doubled around the *Z*-axis (Fig. 7(c)) and has a swing of up to 90° in the orthogonal plane (Fig. 7(d)).

To economise on computation time, the constraints within the leg were reduced to holding adjacent and adjacent-but-one pairs of domains plus, after some initial tests, the separation between the two most distant light-chain domains (18 and 19). With a value of `wild` = 0.01 and a single constraint along the full length of the leg (domains 9–18)[2] this reduced set of constraints was broadly equivalent to the full pairwise inter-domain set of constraints and to test for longer term stability, the simulation was run over 10,000 time steps. This resulted in a stable leg structure that 'wobbled' within a cone with an angle close to 60° in one plane (Fig. 7(f)) and 80° in the orthogonal plane (Fig. 7(f)). Tests were also made extending the long-range constraints from the end of the leg onto the 'ankle' domains (1–19, 7–18). These had the effect of reducing the size of the 'wobble' cone by about half (Fig. 7(h) and (g)).

Values of the true flexibility of the ankle joint are indirect and rare because most biophysical measurements require the myosin to be bound to a substrate and this binding entails flexibility that contributes to any measurement made at the end of the leg. From the close packing of the ankle domain A1 and the first light-chain, it is unlikely that this joint is freely rotating and the variation seen in EM images suggests that flexibility within a cone of up to 90° is possible [16]. Such studies, however, cannot accurately distinguish the orientation of the myosin foot domain and the resulting envelope may contain some rotational averaging about the long axis of the foot. Given this added source of spread, the 70° cone calculated in Fig. 7 is within the expected range of variation.

[2] Because of the tilt of the light-chains, the longest separation along the leg is between domains 9 and 18, rather than 8 and 19 which are the first and last domains in the leg.

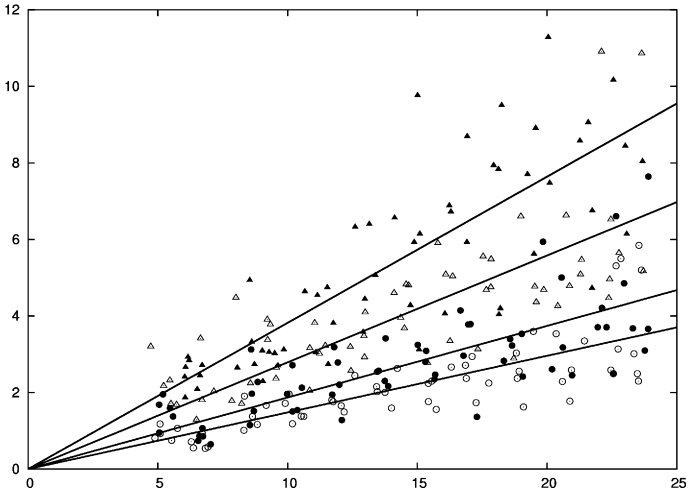

Fig. 8. Myosin leg flexibility. The within-cluster RMS deviation of domain positions (*Y*-axis) are plotted against distance from the foot centroid (*X*-axis) for five runs each of four simulation lengths (in steps): 1000 (open circles), 2000 (filled circles), 5000 (open triangles) and 10,000 (filled triangles). Each data-set can be reasonably fitted by a line passing through the origin (increasing in gradient with increasing run-length) which corresponds to a rigid leg rotating about the centre of the myosin foot.

To estimate whether the distribution within the cone was the result of a rigid or a flexible leg, we plotted the RMS variation of each leg domain against the mean distance from the foot centroid for simulations of different length. Data were collected over five runs for each of 1000, 2000, 5000 and 10,000 steps and by visual inspection, there was a reasonably linear trend with distance from the centroid with no obvious qualitative change with longer simulations (Fig. 8). Before testing this numerically, we estimated the distance from the foot centre about which the leg appeared to rotate by fitting a general line ($ax + b$, where x is the distance from the foot centre) to each data-set. The point at which each line intersects the *X*-axis (i.e., no motion) can be taken as the effective point of rotation. For each data-set, in increasing run-length, these points were: 0.65, −1.16, −2.37, 0.32 (nm), indicating that the foot centroid is a reasonable approximation to a common origin. With this as a fixed point, a more general curve of the form: ax^c was fitted where the value of the exponent (c) gives an estimate of leg flexibility: a straight line ($c = 1$) indicates a rigid leg with higher values of c resulting from excess motion towards the end which can only come from bending. Again in order of increasing run-length, the values of c were: 1.09, 0.93, 0.87, 1.01, none of which constitute a significant deviation from linearity.

3.2. Actin–myosin binding flexibility

3.2.1. Loose binding mode

The myosin loose-binding mode is little more than a proximity constraint and the orientation of the bound myosin is affected only by steric constraints and a bias to have the two actin binding domains (B1 and B2) close to the actin (Section 2.3.1). The effect of these constraints was visualised with a single myosin molecule (plus light-chains) simulated as described above for 10,000 time steps with every tenth coordinate set saved. To separate the actin–myosin inter-molecular component from intra-molecular motions, the random domain and SSE level motion was eliminated and the protein level motion restricted to rotation.

As can be seen from Fig. 9, the loose binding constraint allows sampling over almost a complete sphere with some under-sampling below and along the direction of the actin filament axis caused by actin–myosin steric clashes. There is also some denser sampling towards the starting configuration (top-left in Fig. 9). As the myosin movement has no translational component when bound (except for bump corrections), the range of the distribution is radially symmetric about the centre of the foot domain.

When the Brownian-like motion of the molecule is restored, the radial symmetry is distorted and the foot domain wanders around the actin (Fig. 9(c) and (d)).

3.2.2. Tight binding mode

In the tight binding mode, the myosin binding domains are held at the binding domain of the current actin molecule and tethered to the preceding and following equivalent actin domains (Section 2.3.2). These additional constraints give a preferred orientation aligned with the filament axis (Fig. 10(a)) but have less influence on the position of the myosin viewed down the filament axis, leaving it freer to rotate about the axis (Fig. 10(b)).

Additional constraints were added to restrain this axial rotation of the myosin by introducing links to other neighbouring actin domains across the filament axis. However, these are poorly placed to exert much leverage on the myosin and when given enough strength to do so, they had the undesirable side-effect of disrupting the integrity of the actin chain. Instead, a more direct approach was taken to globally realign the myosin by incrementally moving it to bring its reference frame into alignment with the actin reference frame. This correction was made only about the *X*-axis (filament direction) and the *Y*-axis (the vertical in Fig. 10) leaving the third rotation unrestrained except by local interactions. Under these restraints, the angle of the myosin was seen to drift (over 10,000 steps) from close to 60° under the local constraints to 35° (seen as a blue to red shift in Fig. 10(c)). In the orthogonal direction, however, the wide swing allowed under the local restraints was now greatly reduced (Fig. 10(d)).

3.3. Pre- and post-power-stroke conformations

On ATP binding, the myosin foot adopts an orientation in which it is "tucked" below the leg, forming an acute angle between the long axis of the foot (*X*) and the leg. This conformation is normally referred to as the pre-power-stroke conformation as it is followed by a large conformational change called the "power-stroke" in which the leg and foot return to a more extended conformation, making an obtuse angle between foot and leg. (As shown in all the representations of myosin above.) Coincidentally, the pre-power-stroke conformation is not unlike that of a runner at the start of a race and will be referred to below as the "starting" conformation.[3] Comparing the known structures of myosin-II that adopt both conformations, the angle between the leg positions before and after the power-stroke involves a rotation of approximately 70° [17,18].

This conformational change was modeled as a rotation about the centre of the foot-domain (Section 2.1.3) with the starting conformation specified as the position of the leg when the midpoint of the second light-chain lay on the *Y*-axis of the myosin reference frame. As with the extended conformation (Fig. 10), the equilibrium position of the myosin in this conformation on the actin was evaluated over a simulation of 10,000 steps showing a reasonably isotropic distribution within a small wobble-cone of roughly 10° (Fig. 11).

Combining both starting and final extended myosin equilibrium positions and taking a mean light-chain domain position at the end of each leg gives an angle about the foot centre (close to domain C2) of 75° (Fig. 11(c)). Given the size of the "wobble" cones around each leg, this provides a sufficiently good approximation of the power-stroke movement. As the actin and myosin reference frames are

[3] It should be noted that, unlike its human analogue, myosin sets off backwards out of the starting blocks.

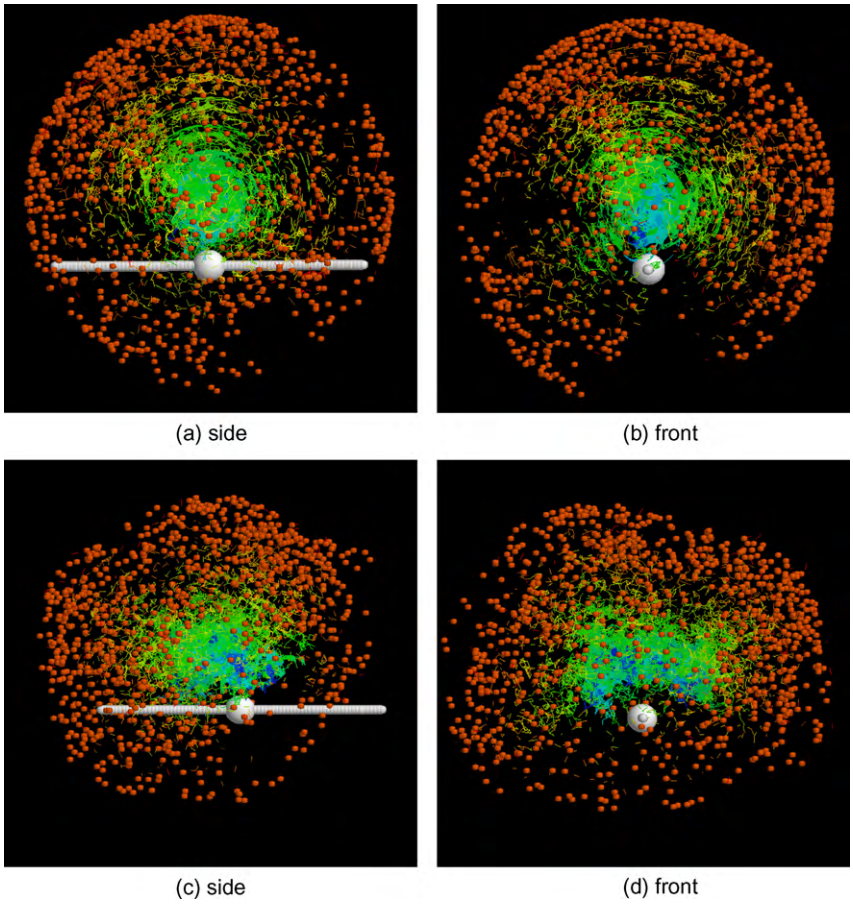

Fig. 9. Myosin loose binding motion. The myosin domain positions are plotted as in Fig. 7 after a 10,000 step simulation from which only one frame in 10 is plotted but as the C-terminal end-points are too scattered to connect as a mesh, they are marked by a small sphere (red). The actin filament axis is indicated by a white tube with a sphere marking the binding position. (a and b) Shows the distribution (as an orthogonal pair) with the myosin foot position fixed and (c and d) shows the distribution when myosin is held in the loose-binding mode. (For interpretation of the references to colour in this figure legend, the reader is referred to the web version of the article.)

restrained to align, the swing of the power-stroke about the myosin *Z*-axis results in a motion in the direction of the actin filament (Fig. 11(d)).

3.4. Myosin dimer flexibility

The starting and final conformations for the myosin monomer described above were extended to model the dimeric molecule, firstly by the addition of a second myosin attached through a freely rotating hinge, followed by the addition of constraints to mimic the steric effect of the cargo and cargo attachment domains and also constraints that may exist as a result of the twofold symmetry of the molecule.

As it is more difficult to follow these wider distributions using the visualisations employed above, their effect will be monitored by the proximity of the unbound myosin foot along the actin filament. Rather than count molecular contacts, a distance-based measure was formulated using a Gaussian function that simultaneously inverts and smooths the actin–myosin distance:

$$\rho_i = \sum \exp\left(\frac{-d_i^2}{\sigma^2}\right), \quad (1)$$

where the density (ρ) of the free myosin foot about each actin (i) is based on the distance of the foot from the actin (d_i) summed over each time-step for a simulation of 1000 steps. (The value of σ will be determined below.) Equivalent densities were also calculated at the domain level.

3.4.1. Estimates from ideal geometry

Without any constraints, the unbound myosin leg can pivot freely about the 'hip-joint' and describes a full sphere about this centre. However, the 'hip-joint' end of the leg of the bound myosin moves over the surface of a sphere within a segment bounded by the extent of the 'wobble' cone described above. The combination of these movements produces a quasi-spherical shell-like distribution (related to a cycloid) that intersects the actin filament axis twice: once at the binding site of the bound leg and again at a distance $2L\cos\theta$, where L is the leg length (20 nm) plus half foot length (2 nm) and θ is the mean angle of the bound myosin leg to the filament (Fig. 12(a) and (b)).

The density (ρ) of the free myosin foot at the filament will depend on the angle theta and as seen above in the simulations, this could lie anywhere between 30° and 60° to the actin filament. We simulated the density distributions for a range of θ from 10° to 60° (Fig. 12(c)). Each plot showed a bimodal distribution with a peak at the origin (referred to as the *proximal* peak) and a second peak (referred to as *distal*) which attained a maximum when $\theta = 20$. If L is 22 nm and θ is around 35°, then the distal peak on the actin filament lies approximately 36 nm beyond the bound actin which corresponds to the separation of the half-period repeat of the actin filament (6.5 actins). However, if theta lies closer to 60° or if the foot is not fully extended then this distance will be reduced.

3.4.2. Freely rotating hinge

The dimer model was simulated with a freely rotating 'hip-joint' and the free myosin foot density was plotted over the filament

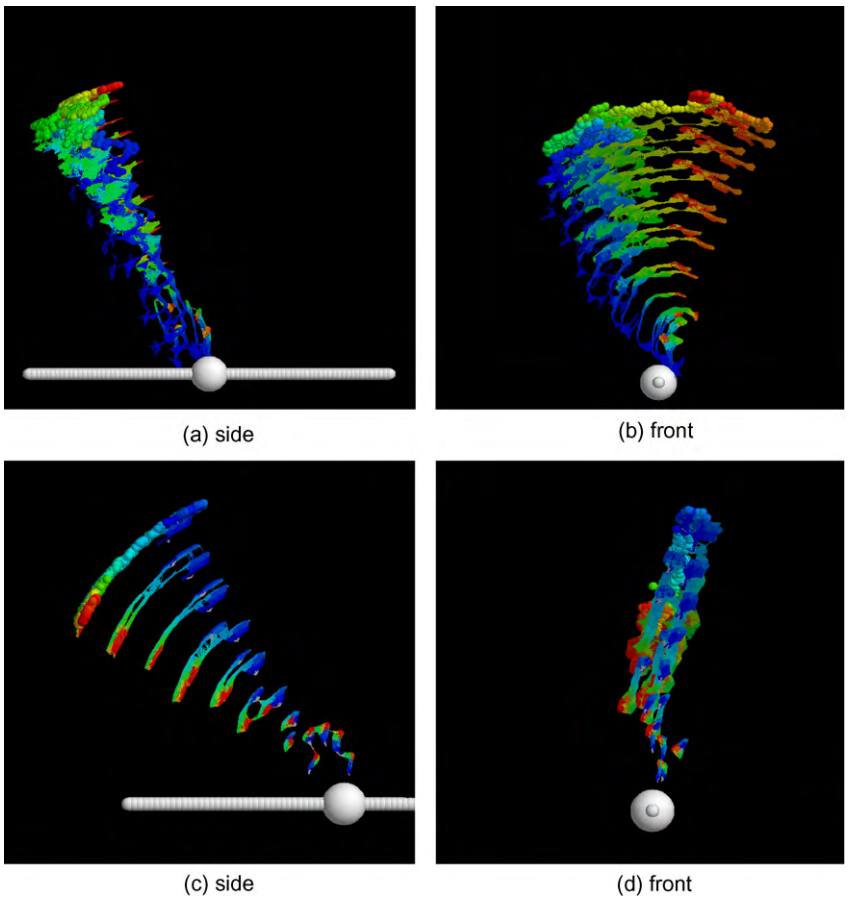

Fig. 10. Myosin tight binding motion on extended foot. The myosin domain positions are plotted as in Fig. 7 after a 10,000 step simulation from which only one frame in 10 is plotted but coloured by time-setup over the course of the simulation (blue = start, red = end). (a and b) Myosin restrained by local actin–myosin interactions. (c and d) Myosin restrained by global (reference-frame) alignment. The myosin foot is in the post-power-stroke (extended) conformation.

length to reveal the expected bimodal distribution with one peak (proximal) set at 0 and the other (distal) 7 actin units beyond (Fig. 12(d)). On the basis of these plots, the value of σ (Eq. (1)) was chosen as 5 nm such that the spread of the two peaks of the distribution matched the theoretical distribution. It can be seen that the distal peak is not as high as the proximal peak. From the numerical simulations above, it can be inferred that this asymmetry is created because the free myosin foot has less freedom when close to the bound myosin compared to the more extended conformation where the wobble of the bound leg is added to its position giving a greater spread of the density and corresponding drop in peak height. When the angle of the bound myosin leg to the filament axis (θ) is 35° the two peaks are equal in height but the distal density quickly drops for values of θ over 35° (Fig. 12(c)). The slight asymmetry in the simulation data was best modelled by $\theta = 37°$, for which the curve is plotted in Fig. 12(d) and others below for reference (see also Supplementary Material for full data).

Steric exclusion was then reintroduced, resulting in a marked drop in the proximal peak height (Fig. 12(e)) with an increased drop in access to the F1 domain (red in the plots) which is currently bound by myosin.

3.4.3. Cargo restricted hinge

If the myosin is attached to a cargo load, this might exert some conformational restriction on the motion of the free myosin leg, either directly or through the smaller but closer cargo attachment domains. The cargo itself is typically a vesicle that is huge in comparison to the myosin (equivalent to a person pulling a house) so we investigated simple ways to mimic its effect that did not involve explicit simulation. We made the simple assumption that the bound myosin will always lie between its cargo and the actin and restrained the free myosin to lie in the hemisphere on the actin side of its distribution. This was implemented by requiring the free myosin to make another random move if its foot domain lay on the forbidden side.

As would be expected, a uniform bias towards the actin makes little difference to the balance between the myosin density at the proximal and distal peak positions, however, the absolute level of occupancy is now three times that seen in the unbiased distribution. The reason it is not simply double reflects steric effects, plus a possible contribution from the Monte-Carlo like resampling algorithm. (Supplementary Fig. 16).

3.4.4. Myosin dimer constraints

The twofold symmetry of the myosin dimer may also affect the distribution of the free myosin along the actin filament. Any bias from this constraint will depend on the nature of the dimer interface which in the myosin-V structure is only partly resolved. Rather than rely on poorly resolved local constraints, the twofold relationship was determined by the *X*-axis of the myosin foot reference frame. When the angle between the two myosin feet fell below 120°, an additional random move was made for the unbound myosin leg. Despite this relatively strict imposition of the twofold constraint, the effect on the myosin densities were minor with only a small increase in the distal peak and a small decrease in the proximal peak (Supplementary Fig. 17(a,b)).

With the addition of the constraint to avoid the direction of the cargo, the two effects of increasing the absolute level of density

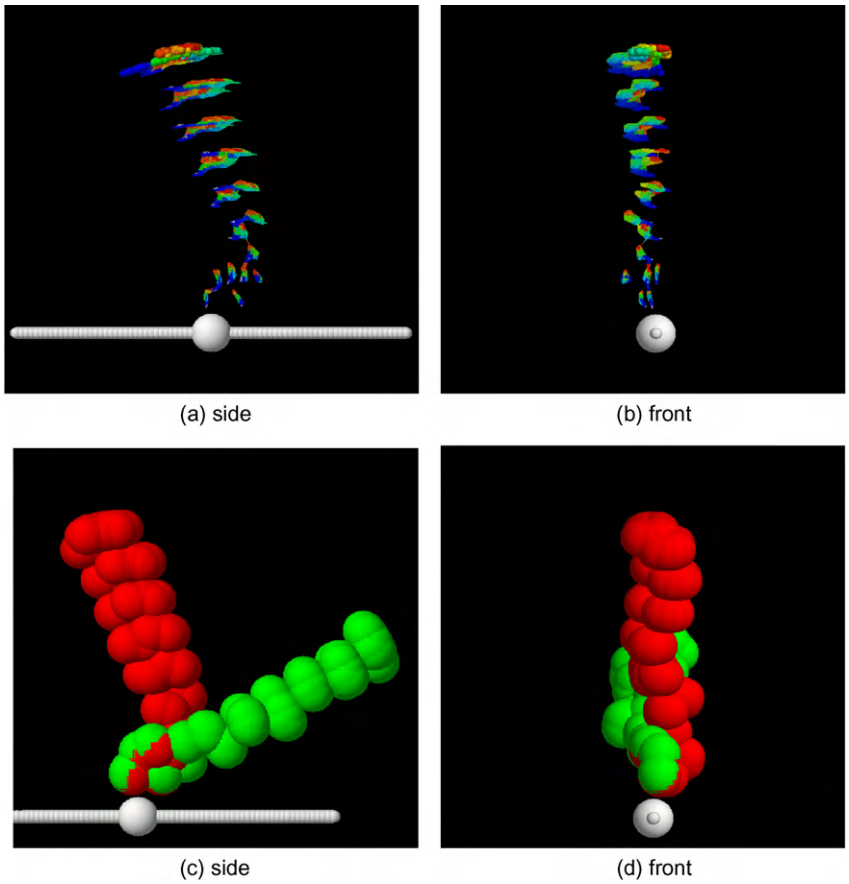

Fig. 11. Myosin tight binding motion on 'starting' foot. The myosin domain positions are plotted as in Fig. 10 after a 10,000 step simulation from which only one frame in 10 is plotted and coloured by time-step. (a and b) Myosin in the pre-power-stroke (starting) conformation under global restraint. (c and d) Combined starting (red) and extended (green) conformations of 96 chains from the end of the simulation, each rendered as domain-sized spheres. (For interpretation of the references to colour in this figure legend, the reader is referred to the web version of the article.)

and the shift of density to the distal peak region were combined giving a strong bias for the free myosin to fall on the region of the filament at actin position +7 relative to the myosin bound actin at 0 (Supplementary Fig. 17(c,d)).

3.5. Pre-power-stroke conformation

The simulations described above were carried out with both myosin molecules in the extended post-power-stroke (extended) conformation. A some point, however, the free myosin will bind ATP and adopt the pre-power-stroke (starting) conformation described in Section 3.3 in which the foot has a more bent-over conformation (likened above to a runner on starting blocks). Similarly, when bound to the actin in this conformation (with associated ATP hydrolysis), there will be a period during which the other myosin leg will release from the actin (with loss of Pi) and be free to explore its conformational space. We simulated both these states and measured the density of the approach of the free myosin foot to the actin filament in the same manner as described above.

3.5.1. Free myosin in the starting conformation

As would be expected, the starting conformation shifts the distal density peak of the free myosin slightly closer to the bound myosin (at position 0). The shift was sufficient to cause a merging of the two peaks measured by the foot-centroid-filament-axis distance and binding domains B2–F1, with only the density associated with the B2–F1′ distance retaining distinct distal and proximal peaks (Supplementary Fig. 18). The position of its distal density peak lies six actin 'units' beyond the bound myosin compared to seven (or 8 to the F1′ domain) for the foot in the extended conformation. Since the F1′ domain at +7 lies close to half a period along the filament axis, both distances are within range of an actin domain in a suitable orientation for binding.

3.5.2. Bound myosin in the starting conformation

As mentioned above, it can be estimated from crystal structures of myosins in the pre- and post-power-stroke conformations that the swing in angle between the leg positions is roughly 70°. The model adopted above for the myosin bound in the extended conformation placed the bound leg at an angle of roughly 35° to the actin filament and a swing of 70° to this places the starting leg just 15° from 'vertical' (i.e., almost orthogonal to the actin filament). This results in a density distribution for the free myosin foot that is markedly different from the bimodal distributions described hitherto with only a single small peak now located close to the origin (Supplementary Fig. 18).

The unexpectedly high density at actin position +1 for the myosin domain B2 approach to the bound actin domain F1 (red in Supplementary Fig. 18) appeared to result from a side-by-side contact, increased by the slightly shorter effective leg-length of the free myosin. The +1 position is too close to the bound myosin for the free myosin to bind which means that until after the power-stroke is made, there is effectively no binding-site available for the free myosin.

4. Discussion

We have described the development and characterisation of a course-grained molecular model for a myosin-V dimer bound to

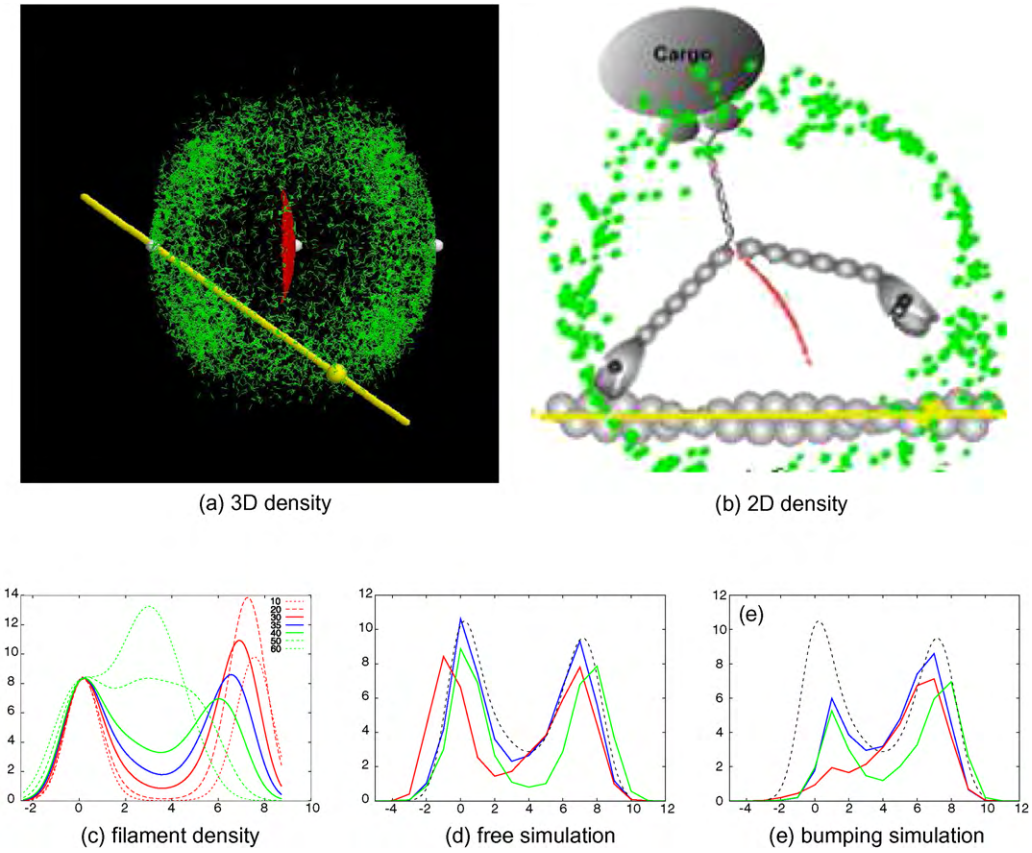

Fig. 12. Theoretical and simulated myosin density plots. (a) The end-points of a jointed rod are plotted with close points 'bonded' to mimic density. The joint is red and the free end is green. White spheres mark, from left to right, the fixed end, the joint at the centre of its range and the extended free end. The line of these points makes an angle (θ) with the actin filament axis (yellow). The data were calculated with $\theta = 35$ and a 'wobble' cone of $\pm 20^\circ$ (RMS deviation). (b) Schematic of the myosin V dimer and actin filament superposed on a slice through the mid-plane of the data in part (a). The red wobble cone is now an arc. The scale of the cartoon components is approximate. (c) The density (*Y*-axis) with which the free myosin foot approaches actin is plotted along the actin filament length (*X*-axis, actins) for the jointed rod (a) with values of θ ranging from 10° to 60°. (See legend on the plot.) The plot for $\theta = 35$ (blue) has equal proximal and distal peak heights. The density of the free myosin foot domain (*Y*-axis) is plotted along the actin filament length (*X*-axis). Density is calculated based on distances from the actin dimer twofold to the foot-domain centroid (blue) and at the domain level from the myosin domain B2 to the bound actin domain F1 (red) and from B2 to actin F1′ (green). (d) The average over the 10 runs. The dashed black curve shows the theoretical distribution for a jointed rod constrained in a similar way to the myosin with $\theta = 37^\circ$ (see Section 3.4.1). The two peaks are referred to as *proximal* (at 0) and *distal*. (e) Plot the equivalent data after the introduction of steric hindrance which results in a drop in density at the proximal peak position. (For interpretation of the references to colour in this figure legend, the reader is referred to the web version of the article.)

an actin filament. This involved the systematic reduction of the known protein structure of myosin-V and its six associated light-chains into secondary structure elements that were then grouped into domains. Constraints between domains were then added to give the molecule a range of flexibility that reproduced that seen in EM images. This approach was extended to the assembly of the actin filament and the components were assembled into a model of a myosin dimer bound to actin.

Simulation of this model with a simple Brownian-like movement allowed the relative motion of the component parts to be investigated. However, because there is no absolute time scale associated with the simulation, only relative movements could be investigated. This was generally done by visualising the density distribution of the components over a fixed number of time steps. Changes in the density after a parameter change or addition of a restraint then allowed the effect of the change to be measured.

4.1. Characterising flexibility

The main aspects of the model that required investigation were the degrees of freedom associated with flexible connections. These included the relative motion of:

- the leg and foot parts of the myosin monomer under both random and directed motion (power-stroke);
- the myosin–actin link under both loose and tight binding;
- the myosin dimer.

4.1.1. Ankle flexibility

With a freely jointed hinge, the flexibility of the ankle (foot–leg) joint was constrained only by the steric interactions of the ankle domains and the first light-chain. As the extended heavy-chain helix was incorporated into the light-chains, this plays no part in the flexibility of the joint. Over a 10,000 step simulation the conformational space explored by the leg motion was equivalent to that estimated from cryo-EM images, spanning a cone with an apex angle of almost 90°. Analysis of this motion indicated that it was best approximated as resulting from a relatively rigid leg with an effective origin of rotation close to the centre of the foot.

4.1.2. Actin binding

Over the same run-length of 10,000 steps in loose binding mode, the leg-wobble plus the binding-wobble extended this cone to cover almost a full spherical range except for a region on the opposite side where the actin filament cast a 'shadow' cone of roughly

90–120°. Similar distributions were obtained both with a free ankle and a 'frozen' ankle.

In tight-binding mode (with a 'frozen' ankle) the myosin was more tightly restrained, holding a position relative to the actin filament close to the starting position at 60°. However, there was greater freedom to swing around the filament axis which was reduced by a global constraint based on the molecular reference frames. Even though the leg-filament angle was not restrained in this way, a shift occurred that reduced the angle to 35°.

4.1.3. Dimer flexibility

The two myosin molecules join at their C-terminal ends as an α-helical coiled-coil. Although the hinge region is poorly resolved, we know from the position of the molecule in its 'docked' conformation that the legs can swing up to almost 180° lying anti-parallel to the coiled coil (Fig. 2). While it is possible that there may be additional constraints associated with a fully loaded cargo, this 'resting' conformation suggests that there is little restriction to performing a full circle swing of the leg in the *X–Y* plane of the actin filament.

Observations of myosin-V 'walking' on a fragment of filament while tethered at the cargo end, indicate that the actin makes a 180° spin per step [19]. Since a full-length filament cannot be spun, this implies that rotation in the *X–Z* actin plane may be more restricted. This restraint was modelled as preserving the twofold symmetry of the dimer but mechanically is likely to involve over and under-twisting of the coiled-coil. If so, it is likely to be independent of motion in the *X–Y* plane.

4.2. Characterising filament access

Anything that aids the search for a new binding site is likely to result in a more effective progress along the filament. From simple geometric considerations, it appears that the free myosin makes its most frequent visits to a suitable binding site when the angle of the bound leg is much lower (35°) than that seen in the cryo-EM structure of the post-power-stroke conformation (60°) where the highest density occurs only three actin units beyond the bound actin. It may be significant that this conformation was based on a muscle myosin that has only two light-chains and therefore a much shorter power-stroke. Although muscle myosin is not processive, artificial processive myosins with two light-chains take steps of this size.

In our simulations, we observed a shift of the leg-filament angle from 60° to 35°. As this rotation was only constrained by local interactions, we believe that this is simply random drift but it does show that there is no steric constraint to prevent a low angle conformation. This means that, even if the foot retains the same binding orientation, there is enough flexibility in the ankle joint for the 35° angle to be accessed, perhaps corresponding to a diffusive phase that has been proposed to complete the step [20]. An additional reason for favouring a lower binding angle for the post-power-stroke conformation is that, given a fixed power-stroke angle, the pre-power-stroke conformation lies at a correspondingly higher angle (that is: more orthogonal to the actin filament). In this position, we found that there was no available actin for the myosin to bind to. Such a situation would reduce any chance of rebinding in the backwards direction.

4.3. Conclusions

Our simulations suggest that a low post-power-stroke angle and high pre-power-stroke angle for myosin-V would lead to more efficient processive motion compared to a more symmetric pair of angles (±60 from orthogonal). Although we found the effect of a twofold symmetry bias to be slight, efficiency would be greatly increased if there was any steric exclusion from the cargo direction, focusing the free myosin down towards the actin.

The model developed and characterised in this study will allow us to develop a more kinetic implementation in which some of the parameters and restraints discussed here can be tested.

Acknowledgements

Z.K. was supported by the Oxford IRC in bionanotechnology and WRT by the Medical Research Council (UK). Justin Molloy and Claudia Veigl are thanked for valuable discussion and comments.

Appendix A. Supplementary data

Supplementary data associated with this article can be found, in the online version, at doi:10.1016/j.jmgm.2010.06.004.

References

[1] T. Hodge, M.J. Cope, A myosin family tree, J. Cell Sci. 113 (2000) 3353–3354.
[2] M.J. Cope, J. Whisstock, I. Rayment, J. Kendrick-Jones, Conservation within the myosin motor domain: implications for structure and function, Structure 4 (August(8)) (1996) 969–987.
[3] J.S. Berg, B.C. Powell, R.E. Cheney, A millennial myosin census, Mol. Biol. Cell 12 (2001) 780–794.
[4] B.J. Foth, M.C. Goedecke, D. Soldati, New insights into myosin evolution and classification, PNAS 103 (2006) 3681–3686.
[5] G.H. Li, Q. Cui, Analysis of functional motions in Brownian molecular machines with an efficient block normal mode approach: myosin-II and Ca^{2+}-ATPase, Biophys. J. 86 (2004) 743–763.
[6] F. Tama, M. Feig, J. Liu, C.L. Brooks 3rd., K.A. Taylor, The requirement for mechanical coupling between head and S2 domains in smooth muscle myosin ATPase regulation and its implications for dimeric motor function, J. Mol. Biol. 28 (2005) 837–854.
[7] W. Zheng, Multiscale modelling of structural dynamics underlying force generation and product release in actomyosin complex, Proteins: Struct. Funct. Bioinfo 78 (2010) 638–660.
[8] Z. Katsimitsoulia, W.R. Taylor, A hierarchic algorithm for simple Brownian dynamics. Comput. Biol. Chem., 34:1–10.
[9] J. Liu, D.W. Taylor, E.B. Krementsova, K.M. Trybus, K.A. Taylor, Three-dimensional structure of the myosin v inhibited state by cryoelectron tomography, Nature 442 (2006) 208–211.
[10] W.R. Taylor, Defining linear segments in protein structure, J. Mol. Biol. 310 (2001) 1135–1150.
[11] W.R. Taylor, Protein structure domain identification, Prot. Eng. 12 (1999) 203–216.
[12] I. Rayment, W.R. Rypniewski, K. Schmidt-Base, R. Smith, D.R. Tomchick, M.M. Benning, D.A. Winkelmann, G. Wesenberg, H.M. Holden, The three-dimensional structure of myosin subfragment-1: a molecular motor, Science 261 (1993) 50–58.
[13] I. Navizet, R. Lavery, R.L. Jernigan, Myosin flexibility: structural domains and collective vibrations, Proteins: Struct. Funct. Bioinfo. 54 (2004) 384–393.
[14] C. Ruff, M. Furch, B. Brenner, D.J. Manstein, E. Meyhöfer, Single-molecule tracking of myosins with genetically engineered amplifier domains, Nat. Struct. Biol. 8 (2003) 226–229.
[15] H. Chen, L.F. Rand Winkler, M.K. Reedy, M.C. Reedy, K.A. Taylor, Molecular modeling of averaged rigor crossbridges from tomograms of insect flight muscle, J. Struct. Biol. 138 (2002) 92–104.
[16] S.A. Burgess, M.L. Walker, H.D. White, J. Trinick, Flexibility within myosin heads revealed by negative stain and single-particle analysis, J. Cell Biol. 139 (1997) 675–681.
[17] M.C. Reedy, Visualizing myosin's power stroke in muscle contraction, J. Cell Sci. 113 (2000) 3551–3562.
[18] R. Dominguez, Y. Freyzon, K.M. Trybus, C. Cohen, Crystal structure of a vertebrate smooth muscle myosin motor domain and its complex with the essential light chain: visualization of the pre-power stroke state, Cell 94 (1998) 559–571.
[19] Y. Komori, A.H. Iwane, T. Yanagida, Myosin-v makes two Brownian 90 degrees rotations per 36-nm step, Nat. Struct. Mol. Biol. 14 (October(10)) (2007) 968–973.
[20] C. Veigel, F. Wang, M.L. Bartoo, J.R. Sellers, J.E. Molloy, The gated gait of the processive molecular motor, myosin V, Nat. Cell Biol. 4 (2002) 59–65.
[21] S. Schmitz, J. Smith-Palmer, T. Sakamoto, J.R. Sellers, C. Veigel, Walking mechanism of the intracellular cargo transporter myosin V, J. Phys.: Condens. Matter 18 (2006) S1943–S1956.